In vivo visualization of butterfly scale cell morphogenesis in *Vanessa cardui*

Anthony D. McDougal[a], Sungsam Kang[b], Zahid Yaqoob[b], Peter T. C. So[a,b,c], and Mathias Kolle[a,1]

[a]Department of Mechanical Engineering, Massachusetts Institute of Technology, Cambridge, MA 02139; [b]Laser Biomedical Research Center, G. R. Harrison Spectroscopy Laboratory, Massachusetts Institute of Technology, Cambridge, MA 02139; and [c]Department of Biological Engineering, Massachusetts Institute of Technology, Cambridge, MA 02139

During metamorphosis, the wings of a butterfly sprout hundreds of thousands of scales with intricate microstructures and nanostructures that determine the wings' optical appearance, wetting characteristics, thermodynamic properties, and aerodynamic behavior. Although the functional characteristics of scales are well known and prove desirable in various applications, the dynamic processes and temporal coordination required to sculpt the scales' many structural features remain poorly understood. Current knowledge of scale growth is primarily gained from ex vivo studies of fixed scale cells at discrete time points; to fully understand scale formation, it is critical to characterize the time-dependent morphological changes throughout their development. Here, we report the continuous, in vivo, label-free imaging of growing scale cells of *Vanessa cardui* using speckle-correlation reflection phase microscopy. By capturing time-resolved volumetric tissue data together with nanoscale surface height information, we establish a morphological timeline of wing scale formation and gain quantitative insights into the underlying processes involved in scale cell patterning and growth. We identify early differences in the patterning of cover and ground scales on the young wing and quantify geometrical parameters of growing scale features, which suggest that surface growth is critical to structure formation. Our quantitative, time-resolved in vivo imaging of butterfly scale development provides the foundation for decoding the processes and biomechanical principles involved in the formation of functional structures in biological materials.

metamorphosis | butterfly scales | biological structure formation | in vivo quantitative phase imaging | cuticle secretion

The functional structures of butterfly wing scales form during pupal development: scale cells grow protrusions that serve as templates for finely sculpted nanoscale cuticle morphologies (1–3). By tailoring these scale morphologies, butterflies produce unique visual appearances (4–7), ensure thermal regulation (8) and water repellency (9), or generate beneficial acoustic (10) and aerodynamic effects (11). Interdisciplinary interest in these material functionalities has led to scientific advances in the comprehensive assessment of the scales' multifunctional material properties (12), design of next-generation bioinspired functional materials (13, 14), identification of key genes in patterning and structural color (15–19), and evaluation of the impact of ecological factors on biodiversity (20, 21). Although the enviable functionality of butterfly wings depends heavily on the precise structural architecture of the wing scales, little is known about the dynamics, processes, and phenomena involved in scale development (22).

Each scale on a butterfly's wing is formed by an individual cell, which secretes a chitinous cuticle that forms a single-cell exoskeleton. In many butterflies, these scales are further organized in rows of alternating cover and ground scale morphologies (1). The mature scales of the painted lady butterfly (*Vanessa cardui*) exemplify a skeletal scale blueprint, which is widely reflected in both the simple and the sophisticated wing scale morphologies found across Lepidoptera (Fig. 1*A–D*). In general, the upper surface of a scale consists of ridges running down its length; these

ridges are composed of overlapping lamellae and are connected by crossribs (23). Supporting trabeculae bridge the upper features and lower scale surface, which is essentially a thin lamina on the order of 100 nm in thickness. The rich diversity of scale morphologies in other butterflies and moths may be thought of as modulations of the basic structures found in this generic scale architecture. Consequently, the easy-to-rear *V. cardui* is a favorable model system for gaining insights into the processes and mechanical phenomena underlying biological formation of functional micro- and nanostructures (15, 24, 25).

Key insights into the formation of these structures have resulted from the analysis of dissected and stained wing tissues at discrete developmental time points. Almost a century ago, the sequence of cellular division, scale protrusion, growth, and ridge formation was documented in flour moths (26). Since then, electron microscopy served to elucidate nanoscale structures in the wing tissue and provided glimpses of cuticle growth on the scale cell (27–29). Seminal studies emphasized the optical function of the scale and offered hypotheses for lamella formation on the scale ridges via mechanical wrinkling (30) and for three-dimensional (3D) structure formation via internal membrane templates (23). This rationale has been used to explain how gyroids and other cubic structures form in scales (31). More recently, confocal imaging has allowed closer examination of
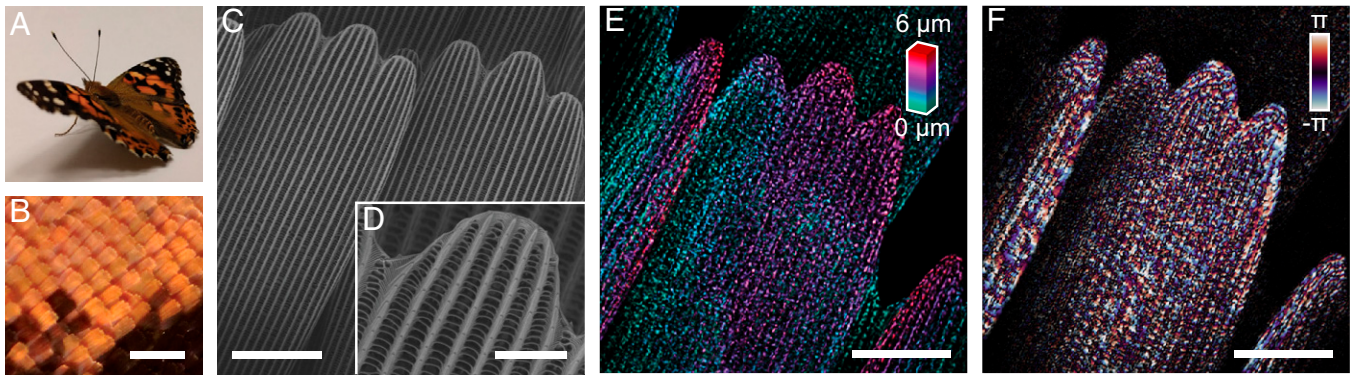
Fig. 1. Imaging the structure of fully formed butterfly scales. (*A*) The painted lady butterfly, *V. cardui*. (*B*) Optical micrograph of orange and black wing scales. (*C*) Scanning electron micrograph of individual adult scales, with ridges running down the length of the scale. (*D*) Magnification of scale finger showing that ridges consist of stacked lamellae and are connected by crossribs. (*E*) Volumetric image of an adult scale acquired by speckle-correlation reflection phase microscopy (red, top of the volumetric data stack; green, bottom). (*F*) A single slice of phase data for the same scale. (Scale bars: *B*, 200 μm; *C*, 20 μm; *D*, 5 μm; and *E* and *F*, 20 μm.)

material distribution, albeit in fixed wing tissues due to a lack of endogenous labeling methods in Lepidoptera. These studies described the signaling factors involved in patterning scale positions (32), explored the role of actin in the formation of scale fingers and ridges (24), and quantified actin bundle spacing and chitin distribution during and after development (25). Together with discrete snapshots from wings fixed at different developmental stages (33), the cuticle structures of mature scales may hint at their formation: in some adult scales, internal gyroids are ordered in increasing size up the length of the scale, possibly illustrating the timing in onset and growth (34).

While these time-discrete imaging efforts provide glimpses into scale development, a comprehensive understanding of the processes underlying scale structure formation can be gained only by continuous observation of the spatiotemporal progression of living scale cells (22). Recent exogenous fluorescent imaging of live lepidopteran pupae captured the young scale cell and the initial protrusion of scales (35, 36). Despite this progress, visualizing subcellular features of live scale cells throughout development remains an unsolved challenge, due to complications inherently associated with the imaging of tissues that feature heterogenous and pronounced micro- and nanoscale refractive index variations. Additionally, imaging over long durations with fluorescent techniques is susceptible to photobleaching and photodamage; moreover, genetic constructs for fluorescent labeling in live organisms are still limited for butterflies.

Here, we report the continuous, in vivo, label-free imaging of developing scale cells in the living *V. cardui* butterfly using speckle-correlation reflection phase microscopy (see Fig. 1 for comparison with scanning electron microscopy data). This quantitative phase imaging technique offers a versatile strategy for observing the growth of functional materials in vivo with high temporal and spatial resolution. We capture critical moments of lepidopteran scale structure formation in living organisms on a continuous timeline. In particular, we identified a two-step process of tissue patterning in the early epithelial sheet and quantified the morphological changes occurring across various length scales as scale cells grow. Insights from continuous imaging of scale formation form the foundation for understanding the biomechanical processes involved in the genesis of functional cuticle morphologies.

Visualization of Scale Features in Live Pupae

To image butterfly wing scales during metamorphosis, we developed a specimen preparation and maintenance protocol that enables in vivo quantitative phase imaging (Fig. 2). We gain optical access to the wing tissue during development by replacing part of the pupa's cuticle with a glass window, exploiting a variety of surgical techniques (Fig. 2 *A* and *B*; see *Materials and Methods* and ref. 35 for timing and techniques). Even macroscopically, wing tissue development can be monitored through the observation window. Initially, the wing is a translucent epithelial sheet; as the scales produce chitinous cuticle, the wing becomes reflective and eventually shows mature pigment patterns (Fig. 2 *B*–*E*). For long-term quantitative observations with high spatial resolution, the optically exposed wing is imaged through the window in the chrysalis using speckle-correlation reflection phase microscopy (37, 38) (Fig. 2*F* and *SI Appendix*, Fig. S1). This interferometric approach yields both phase and amplitude data from live and unlabeled specimens, with excellent axial sectioning, rejecting out-of-focus information (Fig. 2*G* and *I*; *SI Appendix*, Fig. S2; and Movie S1). The amplitude data capture changes in refractive index, which are usually associated with material interfaces (Fig. 2*G*). By scanning through the tissue depth, a three-dimensional image of live, developing scales and wing tissue can be reconstructed for volumes of $75 \times 75 \times 200 \ \mu m^3$ with a maximum lateral resolution of 490 nm and a maximum axial resolution of 1.03 μm. We visualize this 3D volumetric amplitude data by color-coding each data slice according to its height in the image volume (Fig. 2*H* and Movie S2). The phase data capture the height of the material interfaces within each optical slice (*SI Appendix*, Fig. S2). The orientation of the phase gradient, which encodes the local slope at the scale surface, reveals critical scale features (Fig. 2*I*). Individual line profiles quantify the scale surface height with sensitivity to variations on the ~10-nm scale, providing quantitative insights into ridge and lamellae formation throughout scale development (Fig. 2*J* and *K*).

A Phenomenological Timeline of Scale Cell Development In Vivo

We track the development of individual specimens from the first few hours after pupation until the organism begins to eclose; the duration of the pupal stage (100% development) is typically about 10 d and can vary by up to 2 d, with developmental timings dependent on the type of scale and location on the wing (24, 39). We observe the wing tissue as it transforms from a simple folded epithelial monolayer to a mature wing with fully formed scale structures (Fig. 3; Movie S3; and *SI Appendix*, Fig. S3). At around 1% of development, morphologically homogeneous epithelial cells are tightly packed at the wing surface (Fig. 3*A*); they are more sparsely connected on the interior via an evolving network of intercellular junctions (*SI Appendix*, Fig. S4 and Movie S4) that have been previously
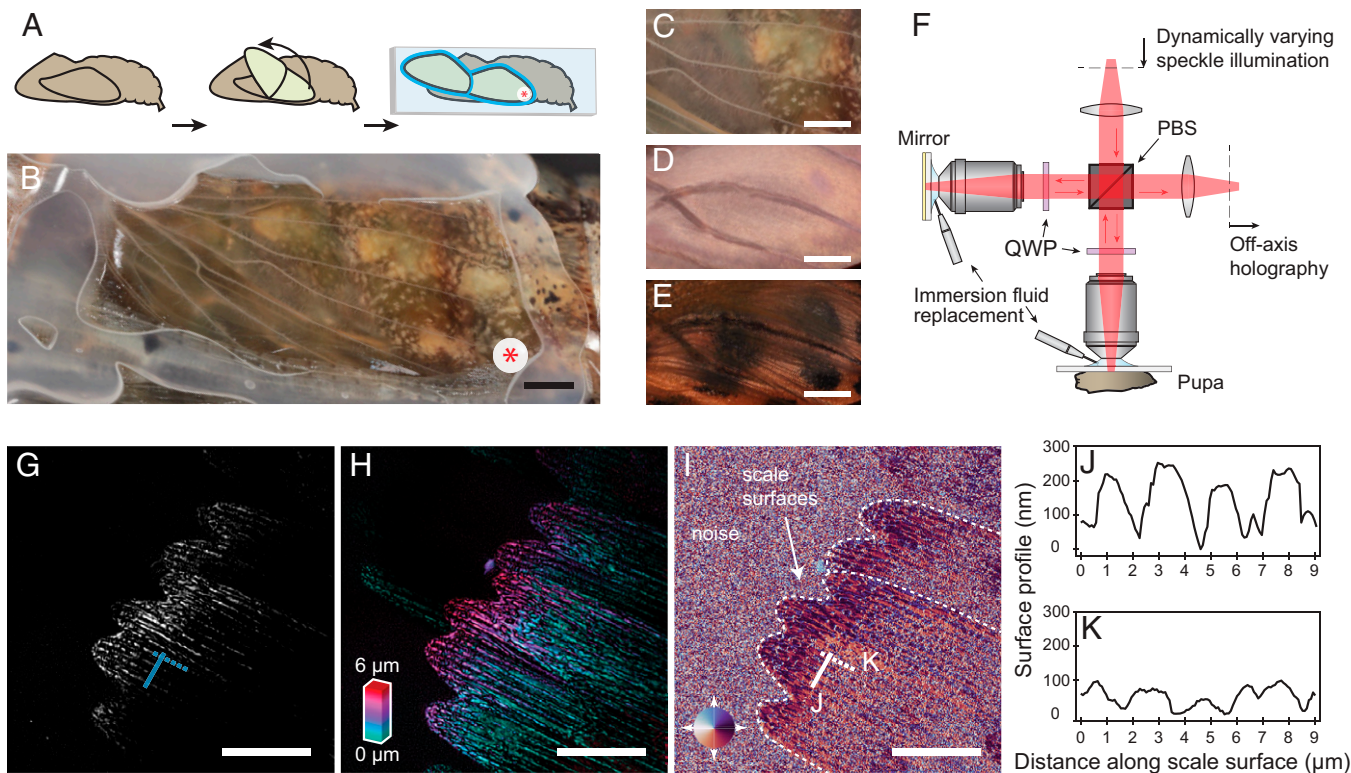
Fig. 2. Optical window and in vivo microscopy to image developing scales. (*A*) Creating an optical window into the chrysalis: lifting a small flap of cuticle and forewing, revealing the hindwing, and sealing of the exposed area with a coverslip and a biocompatible adhesive (blue). (*B*) The exposed wing at 2% of development. The red asterisk marks the location in *A*. (*C–E*) Optically accessible wing area at 3%, 73%, and 100% of development (minutes before eclosion). (*F*) Schematic diagram of the in vivo imaging setup. QWP, quarter wave plate; PBS, polarized beam splitter. (*G*) A single slice of deconvolved reflected light amplitude data, showing the tips of forewing scales in a pupa at 83% development (8.12 d for this specimen). (*H*) Volumetric amplitude stack showing overlapping scales (red, highest slice; green, lowest slice through a 6–μm depth). (*I*) Visualization of micro- and nanoscale features on scales via the phase gradient associated with the amplitude data in *G*. The colored cone indicates the tilt orientation (red, southward; blue, northward downhill slope). (*J* and *K*) Surface profiles along lines indicated in *G* showing ridges (*J*) and height of ridge lamellae (*K*). (Scale bars: *B–E*, 1 mm; *G–I*, 20 μm.)

Scale-Forming Processes Implicated by Morphological Dynamics

described as feet and cytonemes (36, 40). Mitoses of generalized epidermal cells are readily seen occurring in-plane with the tissue (Movie S4). Then, select cells–the scale precursor cells–swell in size (red regions in Fig. 3*B*). These cells undergo two divisions: after the first division, one daughter cell degenerates, while the other continues to the second division to produce a scale cell and a socket cell (*SI Appendix*, Fig. S5) (26). The scale cell protrudes through the socket, away from the wing surface (Fig. 3*C*). Although the membrane of the protrusion is initially rough–likely due to microvilli that underlie epicuticle formation (27, 29)–the surface soon becomes smooth (*SI Appendix*, Fig. S6). The scale then expands (Fig. 3*D*), ultimately reaching its final length and width before 60% of pupal development. As the scale reaches its final length, the leading edge splits into fingers and the longitudinal structure of ridges appears (Fig. 3*E*). In previous studies, scanning electron microscopy has shown that procuticle–a matrix of chitin and protein–grows at these ridge locations (27, 29). The ridges become more defined and develop lamellae, while the lower lamina gradually expands to cover all but the edges of the lower surface (Fig. 3*F*).

Scale-Forming Processes Implicated by Morphological Dynamics

By tracking gradual changes in scale growth over time, we can explicitly define the timing of specific developmental events within individual pupae and begin to understand the processes guiding morphogenesis (Fig. 3*G*). Here, we address two aspects of wing scale development: spatial patterning of the scale precursor cells

in the wing tissue and evolution of scale ridge spacing and height during scale growth.

Scale Precursor Cells of Cover and Ground Scales Differentiate in a Row at Two Separate Times. In *V. cardui* and other butterflies, scales are arranged in neat rows, with alternating ground and cover scales. The first step in this patterning has been attributed to lateral inhibition via the Notch signaling pathway, which leads to loose rows of isolated precursor cells. This attribution is based on a comparison with *Drosophila* bristle development, where Notch signaling between neighboring cells creates a feedback loop that results in spatially isolated, low-Notch cells that become bristle precursor cells (32, 41, 42). Likewise, in the wings of young lepidopteran pupae, cells with low Notch expression have been observed in a loose row-like pattern (32). The manner in which scale precursor cells are organized into their final neat row pattern has not yet been determined, although cell migration and rearrangement have been proposed as hypotheses (32, 40). Very little is known about when and how a precursor cell transitions to a ground or a cover scale.

Our data in *V. cardui* show that a subset of epithelial cells differentiates into loose rows of large, isolated precursor cells (Fig. 4*A*), in agreement with previous observations of early morphological differentiation (32, 39, 40). Although these precursor cells are initially only roughly aligned, they subsequently shift into more defined rows (Fig. 4*B* and *C*) without touching each other. Then, the smaller cells that are positioned between the precursor cells also differentiate, growing to the large precursor cell size (Fig. 4*C* and *D* and Movie S5). Since the first and second sets of precursor cells alternate down a given row, each group must give

McDougal et al.
In vivo visualization of butterfly scale cell morphogenesis in *Vanessa cardui*

PNAS | 3 of 8
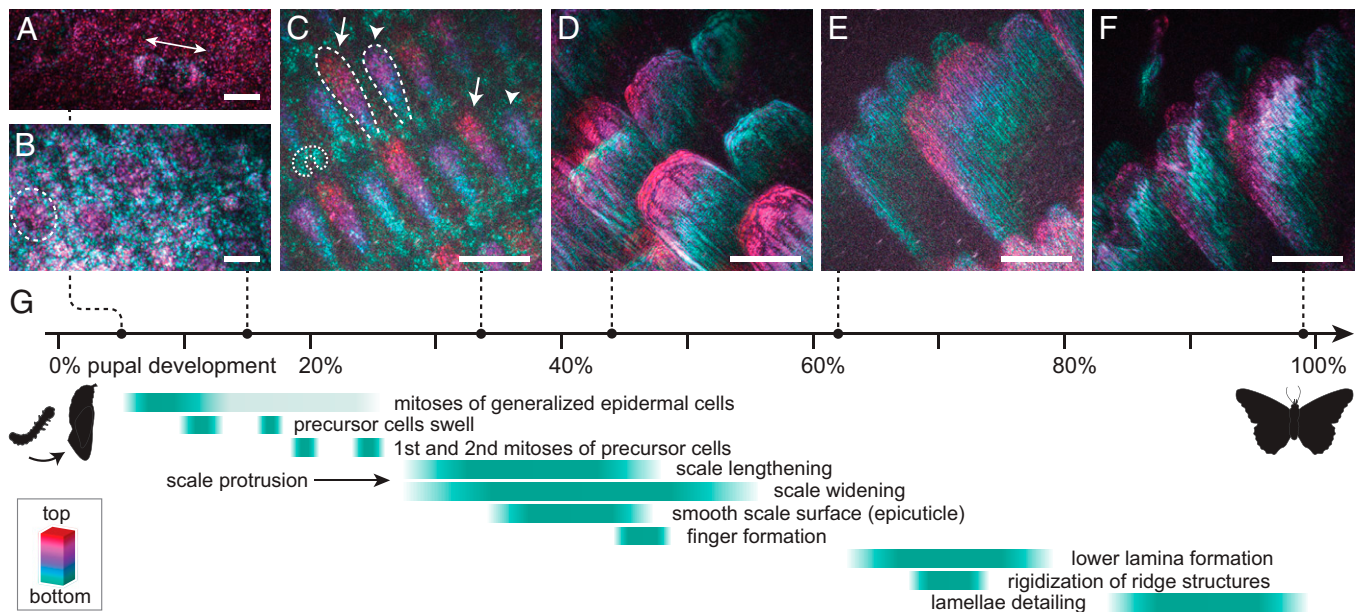https://doi.org/10.1073/pnas.2112009118

Fig. 3. Continuous imaging of scale growth on an individual *V. cardui* pupa. (*A*) Wing tissue at 5% of pupal development, exhibiting cell division prior to precursor cell differentiation. (*B*) Enlarged, raised precursor cells (red, encircled by dashed line) are identifiable at 15% development. (*C*) Scales (two are emphasized by the dashed outlines) have begun to grow away from the sockets on the wing (one is emphasized by the dotted outline) at 34% development; cover scales (arrows) and ground scales (arrowheads) are easily distinguishable. (*D*) Expanding scales and the beginning of finger formation at 44% development. (*E*) Scales at their final size with well-pronounced fingers at 62% development. Longitudinal structures are faintly visible. (*F*) Scales show a lower lamina (green zone) underneath developed ridges (red zone) at 99% development. (*G*) Timeline of significant events observed in developing tissue, allowing for variation between wing locations. Shown beneath *G* is the representative color bar indicating volumetric image depth for all images: 0 μm to 6 μm (*A*, *B*, and *D–F*) and 0 μm to 16.8 μm (*C*). (Scale bars: *A* and *B*, 10 μm; *C–F*, 20 μm.)

rise to either cover or ground scales. Once the scales grow and the shapes of ground and cover scales are distinguishable, we can follow them back in time to determine their relative positions. The distal position and late appearance of the second set suggest that they are ground scale precursor cells, and the first set are the cover scale precursors (*SI Appendix*, Fig. S7).

Thus, the formation of tight rows of scales is primarily enabled by the differentiation of a second set of scale precursor cells
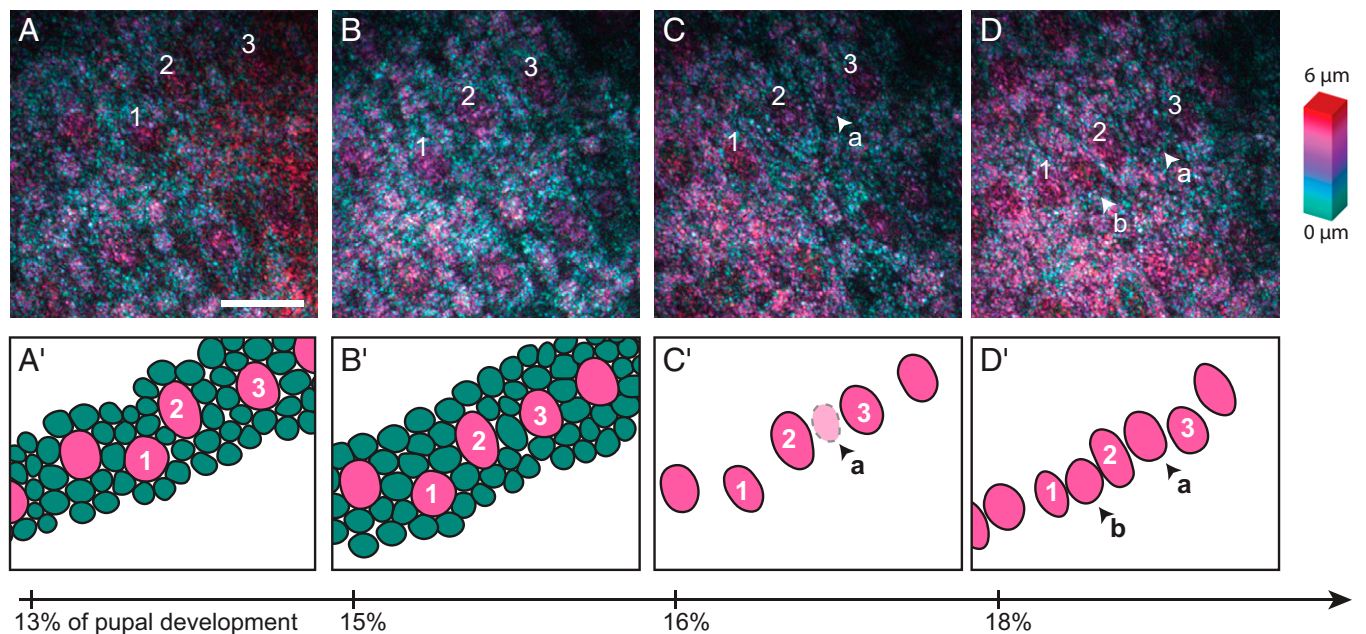

Fig. 4. Scale precursor cells appear in two stages. Cover scale precursor cells (raised red spheroids) are labeled 1, 2, and 3 and are tracked over 13 to 18% of development in a single pupa. (*A*) Precursor cells initially align roughly in rows. (*B*) Same precursor cells slightly shifted. (*C*) A new precursor cell (arrowhead "a") begins to enlarge between cell 2 and cell 3; all the precursor cells move toward greater alignment. (*D*) New ground scale precursor cells (arrowheads) are now of comparable size to the older ones; all precursor cells are arranged in a straight row. (*A'–D'*) Schematic depiction of the precursor cells (magenta). Note that borders of the surrounding cells (green) are not clearly discernible everywhere in the data but are drawn only for illustrative purposes. Volumetric image depth: 0 to 6 μm. (Scale bar: 20 μm.)

that spatially alternate in line with the first set. What determines the spatial positioning and timing of differentiation for this second set of precursor cells? In the development of *Drosophila* bristles—which have frequently been described as homologous to lepidopteran scales (24, 32)—lateral inhibition behavior of Notch dynamics can generate temporary stripe patterns of contiguous cells evolving into a row of nonadjacent bristle precursor cells (42). Yet our data show that the first group of scale precursor cells is already nonadjacent in *V. cardui*, similar to the Notch pattern on *Heliconius erato* butterflies (32).

Scale Ridges Develop at Constant Spacing. To identify geometric constraints and infer biomechanical processes that influence the morphological development of scales, we tracked and quantified the evolution of various structural parameters in vivo in individual butterflies (Fig. 5; note that the precise time of scale development may vary, and the scales in Fig. 5 developed slightly sooner than those shown in Fig. 3 but followed the same progression of events). A relatively short window of time, roughly 35 to 40% of development (around 100 h to 114 h), contains many key moments of scale formation: the scale reaches its maximal size, fingers form, and ridges appear (Fig. 5*A* and *B*). Scale length and width develop on different timelines, with the length retracting slightly even before the scale reaches its terminal width (Fig. 5*C* and *D*). During much of scale expansion, the already-slender scale gradually continues to thin (Fig. 5*E*). Yet, despite this anisotropic growth, estimates of scale volume and surface area grow in lockstep (Fig. 5*F*).

At ∼39% of development, long spars of material running down the length of the scale become visible in the amplitude data (Fig. 5*G*). Since the phase data show a smooth scale surface when these features first appear, these spars are likely bundles of actin that will eventually template the ridges, as has been described previously (24, 25, 28). As the scale widens, the spacing of actin bundles also widens until it reaches ∼1.8-μm separation. Soon after, the surface of the membrane is no longer smooth, and it becomes difficult to determine whether the longitudinal striations in the amplitude data are the actin serving as ridge templates or the ridges themselves. Previous work suggests that actin bundle spacing and cuticular ridge spacing are tightly related and appear to not change from 40 to 95% development (25). We tracked this spacing on individual scales in our continuous data and confirmed that after the scale surface is no longer smooth, the periodic spacing indeed remains constant on individual scales through the vast majority of ridge development (for the measured scales, at least until 89% of pupal development).

Our phase data reveal how surface morphology changes at the onset of ridge formation (Fig. 5*H* and *SI Appendix*, Fig. S8). The epicuticle on the scale surface is smooth during most of the scale expansion. The onset of ridge formation appears to start near the end of the scales' expansion (∼37% of development for this specimen), after the scale has reached its maximal length but before it has attained its full width. Undulations in surface height appear, but with irregular spacing and varying distribution across the scale's surface. This spatial and temporal heterogeneity may be due to variations in the onset of cuticle production. Then, at ∼39% development, periodicity becomes highly regular and remains regular as the nascent ridges grow in height. Phase and amplitude data together indicate that ridge spacing remains nearly constant from the earliest moments of
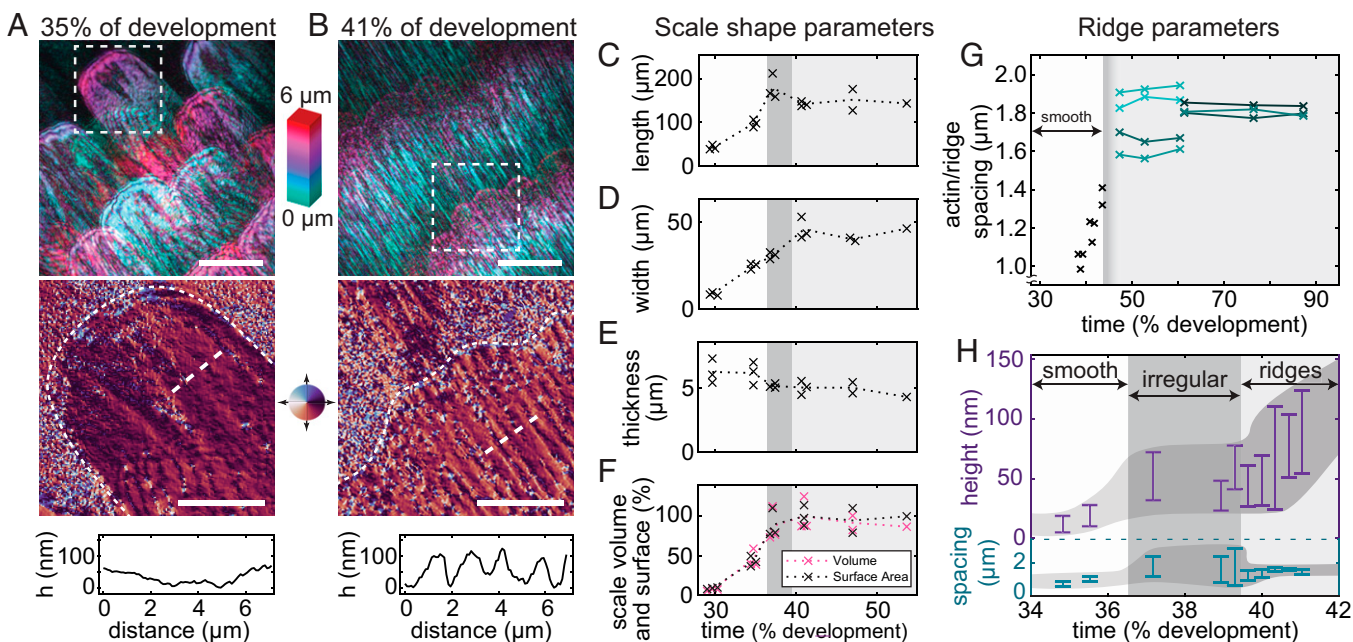

Fig. 5. Quantification of scale shape evolution and ridge growth. (*A*) Scale morphology at 35% of pupal development. Volumetric data (*Top*) show midsized scales. Phase data (*Middle*) from the region marked in the volumetric data and a height profile (h) of the phase data (*Bottom*) taken along the white dashed line indicate a relatively smooth scale surface. (*B*) Scale morphology at 41% of pupal development. Scale fingers are apparent in volumetric data. Phase data (*Middle*) from marked region indicate regular spacing of proto-ridges, which are about 100 nm in height (bottom profile extracted from dashed line). (*C*–*F*) Measured and mean scale shape parameters during development: length (*C*), width (*D*), thickness (*E*), and volume (red) and surface area (black) as percentage of maximum estimated from the bounding box of scales (*F*). Shaded time spans are specified in *H*. (*G* and *H*) Ridge parameters during development: spacing between forming ridges for multiple scales (*G*). Each curve of connected data points shows continuous measurements of an individual scale. (*H*) Characterization of ridge height (purple) profiles and ridge periodicity (teal). Bars indicate SD; curve outlines qualitatively illustrate general feature development. White background marks the time span when the scale surface is rather smooth; dark gray shading indicates the time span where forming structures are irregular and spacing distribution varies; light gray indicates the time span when periodicity of the ridges is determined and height grows. Data in *A*–*F* and *H* were acquired from a single pupa; for *G* a different pupa was used to follow ridge development on single scales over longer periods of time. Error bars correspond to measurements from three scales. Volumetric image depth: 0 to 6 μm. (Scale bars: *A* and *B*, *Top*, 20 μm; *A* and *B*, *Middle*, 10 μm.)

McDougal et al.
In vivo visualization of butterfly scale cell morphogenesis in *Vanessa cardui*

PNAS | 5 of 8
https://doi.org/10.1073/pnas.2112009118

ridge appearance and growth until late in scale development, when much of the ridges' fine structure has been established; we have not yet determined whether there are any spacing changes after 89% development through eclosion and the drying of the scales.

Other studies have shown that ridges appear between regularly spaced bundles of actin filaments (25, 28), which are necessary for proper ridge formation (24). As ridges grow, they develop their fine lamellar structure. One hypothesis, established almost 40 y ago, proposes that lamellar formation is a wrinkling phenomenon driven by mechanical buckling of the cuticle layer with the required stress arising from a decrease in distance between the actin bundles (30).

However, our data indicate that ridge spacing remains constant after initial ridge appearance, implying that a decrease in actin bundle spacing is unlikely and thus cannot drive ridge formation. Nevertheless, buckling remains a plausible mechanism for the formation of ridges and lamella, potentially resulting from growth of the scale surface subject to an underlying mechanical constraint. The growing surface area of membrane and deposited cuticle may be spatially constrained by the actin bundles, leading to out-of-plane buckling; alternatively, differential growth between the membrane and cuticle might lead to stresses that induce ridge appearance (43). Further studies are needed to reveal the biomechanical phenomena underlying the interplay of actin, cell membrane, and deposited cuticle that drive the formation of the scale ridge structures.

Conclusion

Using speckle-correlation reflection phase microscopy and lepidopteran surgical techniques, we demonstrate label-free continuous visualization and quantitative characterization of microscale structure formation in live lepidopterans, gaining quantitative insights about cellular organization and development of subcellular features on single scales throughout pupal development. At the tissue level early in development, we observed the sequential patterning of precursor cells for cover and ground scales. Our observations raise questions about the signaling that enables ground scale differentiation, since previous work indicates that the first set of precursor cells exhibits low Notch and represses scale-forming transcription factors in its neighbors (32, 42), which includes the second set of precursor cells. Further studies are required to understand how the ground scale pattern is organized between the cover scales. At the single-cell level, our quantification of the spacing and height of scale ridges reveals that the ridge spacing remains constant from the first occurrence of ridges at about 47% development to at least 89% development. This suggests that the formation of ridges is unlikely to result from a reduction in actin bundle spacing as hypothesized in earlier work (30), yet may be driven by surface growth and buckling when constrained by the actin bundles. Future studies with our imaging approach may further characterize scale material growth and inform quantitative mechanical models that are needed to ascertain the biophysical mechanisms underlying the formation of the scales' fine ridges and crossribs. We anticipate that our imaging strategy may accelerate developmental studies in other species of Lepidoptera or even other orders, since it bypasses the need to develop endogenous labeling or sustained exogenous labeling. The progression of scale structure formation in *V. cardui* is likely to have significant parallels to other lepidopterans. A comparison between the scale structures of different species and their respective development timelines will help identify the processes responsible for creating and fine-tuning structural features. Future work on pushing the limits of resolution of the presented phase imaging approach, quantitative mapping of refractive index distribution, and standardization of key system components may facilitate the implementation of our approach in other studies of biological material formation and cellular

and tissue development. Additionally, our in vivo imaging may be used in conjunction with genome editing protocols (15, 16) or molecular inhibition (24) to elucidate genetic and molecular mediators of structure formation. We consider label-free quantitative phase imaging on whole living organisms an essential tool in the quest for shedding light on the interplay of genetics, proteomics, and biomechanics to enable structure phenotypes with specific functionality. Insights into the formation principles of the multifunctional material structures employed by insects may also allow us to glean specific manufacturing strategies with control over material architecture across all functionally relevant length scales.

Materials and Methods

Butterfly Rearing. Painted lady (*V. cardui*) butterflies were raised in our laboratory with original stock obtained from Carolina Biological Supply Company. Larvae are monitored in individual containers to identify the time of molting of the larval skin to within 15 min. The percentage of development of an individual after surgery is estimated using the average duration of pupal development of other pupae from the same generation. Additional details are included in *SI Appendix*.

Pupal Surgery. We use two surgical approaches to expose the forewing and hindwing tissue in the chrysalis, respectively. To expose the forewing for single time point imaging (Fig. 2*A*), we remove part of the cuticle from above the forewing. This cuticle can be removed at any time after apolysis, which occurs at ∼20% of development (*SI Appendix*, Fig. S3). We anesthetize the pupa in a small chamber that has been flushed with carbon dioxide for 5 to 10 min to immobilize the organism while making a small (∼1 × 1 mm), shallow cut in the chrysalis with a scalpel (Feather; Micro Scalpel) to remove the cuticle. We then place a 150 μm-thick (VWR; no. 1) glass coverslip over the exposed tissue and seal it with a light-curing dental composite (Pentron; Flow-It ALC) using a handheld dental curing lamp (NSKI; LY-02 LED Light Cure Lamp).

To expose the hindwing for continuous imaging, we adapted the surgical strategy described by Otaki and coworkers (35, 44). We grasp the chrysalis cuticle of a recently molted pupa together with the forewing and fold it anteriorly toward the head (these younger pupae do not require immobilization). To limit the spread of any potential melanization immune response, we separate the hindwing from the forewing with a strip of dental composite. Again, we placed a glass coverslip over the exposed wing and sealed it with dental composite. Additional details are included in *SI Appendix*.

Speckle-Correlation Reflection Phase Microscopy. We employ the interferometry technique previously published (37, 38) (*SI Appendix*, Fig. S1). Briefly, a supercontinuum laser (NKT Photonics; SuperK Extreme EXR-4) is sent through a rotating diffuser to produce a dynamically varying speckle illumination. With a bandpass filter, center wavelength 800 nm is chosen with 40 nm bandwidth. The illumination is then distributed with a polarizing beam splitter to the objectives (Olympus; LUMPLFLN 60XW, 1.0NA water dipping) on the reference arm and the sample arm; quarter-wave plates cause the reference and sample signal polarizations to remain orthogonal to each other. Off-axis holography is achieved by means of a grating to divide the combined signals, followed by a combination of polarizers and quarter-wave plates to filter and align the signals for interference. The interferogram is then captured by a camera (Point Gray; Flea3) with up to 100 fps speed and processed in Fourier space to gather the amplitude and phase information from the sample. A motorized stage in the sample stage scans the vertical position of the sample to acquire a volumetric image. The theoretical lateral resolution of 490 nm and the theoretical axial resolution of 1.03 μm were previously corroborated with measurements (37). When imaging beneath a surface in vivo, the resolution is expected to be lower due to multiple scattering and spherical aberration from the tissue and potentially may also gradually degrade over time if the reference arm drifts.

Imaging Protocol. We typically begin to image the pupa within 1 h to 3 h after surgery. We place the pupa under the reference arm of the speckle-correlation reflection phase microscope and scan along the optical axis (*z* axis) in 400-nm steps to build up a volume of image slices. Appropriate imaging depth is algorithmically determined by locating the depth of maximum area-integrated intensity. The reference arm is adjusted to match the change in optical path length. A coverslip with a reflective gold coating on the far side is used as the reference mirror to cancel the dispersion and path-length delay introduced by the pupa's coverslip.

For continuous imaging, a program automatically cycles through the focusing and image acquisition process every 15 min, with microscope alignment checked in person once per day; a syringe pump periodically replaces water lost by evaporation at the immersion lenses. For single time point images (e.g., Fig. 2G–J), carbon dioxide is flowed over the pupa for 5 min to ensure immobilization immediately prior to imaging. Computation and interface control were executed using MATLAB (MathWorks). Additional details are included in *SI Appendix*.

Data Processing and Visualization. We found that 10 iterations of Lucy–Richardson deconvolution with the theoretically estimated point spread function (45) are effective for visualizing scale features in the amplitude data, particularly in middle- to late-stage scale structures (Figs. 1 and 2).

The color representations of 3D amplitude data are based on the Temporal-Color Code plugin by Kota Miura for Fiji/ImageJ. Image slices are colored according to their depth position, and then an average intensity is taken along the volume depth for each RGB channel.

The initial phase data are wrapped on 2π, which can be described as

$$\phi_{\text{wrapped}} = W\phi_{\text{unwrapped}}, \qquad [1]$$

where W is an operator for wrapping, given by

$$W\phi(n) = \phi(n) + 2\pi k(n) \qquad [2]$$

with $k(n)$ as an integer that ensures wrapping; i.e., $-\pi < W\phi(n) \leq \pi$. Itoh (46) described the unwrapping process for $n = 0, 1, \ldots, N$ points of wrapped phase data $-\pi < \phi_{\text{wrapped}}(n) \leq \pi$ in one dimension:

$$\phi_{\text{unwrapped}}(m) = \phi_{\text{wrapped}}(0) + \sum_{n=1}^{m}\left(W\Delta\phi_{\text{wrapped}}(n)\right), \qquad [3]$$

where Δ is an operator for the differential, $\Delta\phi(n) = \phi(n) - \phi(n-1)$. We use this approach to analyze 1D profiles in our phase data.

In 2D, unwrapping can suffer from the effects of noise and cliffs, which are compounded when considering both dimensions (47). We represent the local phase behavior via the integrand of the unwrapping scheme,

$$W\Delta\phi_{\text{wrapped}}(n), \qquad [4]$$

which represents the local phase gradient along a particular dimension. Combination of the horizontal and vertical components of this gradient allows us to determine the direction of slope of the surface. This visu-

alization strategy allows discernment of fine features in the midst of much larger depth changes. Additional details are included in *SI Appendix*.

Image Analysis. We use Dragonfly (Object Research Systems) to measure length, width, and thickness of cover scales in deconvolved 3D amplitude data (*SI Appendix*, Fig. S9). Length was extrapolated for scales that lay partly outside the imaging window (*SI Appendix*). Surface area and volume are estimated using the measured length, width, and thickness to define the presumptive bounding box of the scale.

To measure ridge height and spacing in the phase data (*SI Appendix*, Fig. S10), we unwrap and rotate a 1D profile from a slice of phase data. We find the dominant spatial frequency via Fourier analysis. We define the height of the peak as the distance from the peak to the line connecting the troughs on either side of the peak. The mean and SD peak height are calculated for each profile; all profiles are then used to determine the pooled mean and the pooled SD for each time point.

To measure the actin/ridge spacing in the amplitude data (*SI Appendix*, Fig. S11), we first rotate the data to capture the plane of a scale and define the region of interest of a scale in Dragonfly. We then find the dominant spatial frequency via 2D Fourier analysis. Additional details are included in *SI Appendix*.

1. H. F. Nijhout, *The Development and Evolution of Butterfly Wing Patterns* (Smithsonian Institution Scholarly Press, Washington, DC, 1991).
2. A. McDougal, B. Miller, M. Singh, M. Kolle, Biological growth and synthetic fabrication of structurally colored materials. *J. Opt.* **21**, 073001 (2019).
3. W. O. McMillan, L. Livraghi, C. Concha, J. J. Hanly, From patterning genes to process: Unraveling the gene regulatory networks that pattern *Heliconius* wings. *Front. Ecol. Evol.* **8**, 221 (2020).
4. H. Ghiradella, Light and color on the wing: Structural colors in butterflies and moths. *Appl. Opt.* **30**, 3492–3500 (1991).
5. P. Vukusic, J. R. Sambles, Photonic structures in biology. *Nature* **424**, 852–855 (2003).
6. B. D. Wilts, M. A. Giraldo, D. G. Stavenga, Unique wing scale photonics of male Rajah Brooke's birdwing butterflies. *Front. Zool.* **13**, 36 (2016).
7. D. G. Stavenga, H. L. Leertouwer, K. Arikawa, Coloration principles of the great purple emperor butterfly (*Sasakia charonda*). *Zoological Lett.* **6**, 13 (2020).
8. C. C. Tsai *et al.*, Physical and behavioral adaptations to prevent overheating of the living wings of butterflies. *Nat. Commun.* **11**, 551 (2020).
9. S. Kim, Z. Wu, E. Esmaili, J. J. Dombroskie, S. Jung, How a raindrop gets shattered on biological surfaces. *Proc. Natl. Acad. Sci. U.S.A.* **117**, 13901–13907 (2020).
10. T. R. Neil, Z. Shen, D. Robert, B. W. Drinkwater, M. W. Holderied, Moth wings are acoustic metamaterials. *Proc. Natl. Acad. Sci. U.S.A.* **117**, 31134–31141 (2020).
11. N. Slegers *et al.*, Beneficial aerodynamic effect of wing scales on the climbing flight of butterflies. *Bioinspir. Biomim.* **12**, 016013 (2017).
12. T. B. H. Schroeder, J. Houghtaling, B. D. Wilts, M. Mayer, It's not a bug, it's a feature: Functional materials in insects. *Adv. Mater.* **30**, 1705322 (2018).
13. V. Narasimhan *et al.*, Multifunctional biophotonic nanostructures inspired by the longtail glasswing butterfly for medical devices. *Nat. Nanotechnol.* **13**, 512–519 (2018).
14. Q. Shen *et al.*, Butterfly wing inspired high performance infrared detection with spectral selectivity. *Adv. Opt. Mater.* **8**, 1901647 (2020).
15. L. Zhang, A. Mazo-Vargas, R. D. Reed, Single master regulatory gene coordinates the evolution and development of butterfly color and iridescence. *Proc. Natl. Acad. Sci. U.S.A.* **114**, 10707–10712 (2017).
16. Y. Matsuoka, A. Monteiro, Melanin pathway genes regulate color and morphology of butterfly wing scales. *Cell Rep.* **24**, 56–65 (2018).
17. M. N. Brien *et al.*, Phenotypic variation in *Heliconius erato* crosses shows that iridescent structural colour is sex-linked and controlled by multiple genes. *Interface Focus* **9**, 20180047 (2019).
18. R. C. Thayer, F. I. Allen, N. H. Patel, Structural color in *Junonia* butterflies evolves by tuning scale lamina thickness. *eLife* **9**, e52187 (2020).
19. V. J. Lloyd, N. J. Nadeau, The evolution of structural colour in butterflies. *Curr. Opin. Genet. Dev.* **69**, 28–34 (2021).
20. S. M. V. Belleghem *et al.*, Complex modular architecture around a simple toolkit of wing pattern genes. *Nat. Ecol. Evol.* **1**, 52 (2017).
21. E. J. Tan, B. D. Wilts, B. T. K. Tan, A. Monteiro, What's in a band? The function of the color and banding pattern of the banded swallowtail. *Ecol. Evol.* **10**, 2021–2029 (2020).
22. B. D. Wilts, P. L. Clode, N. H. Patel, G. E. Schröder-Turk, Nature's functional nanomaterials: Growth or self-assembly? *MRS Bull.* **44**, 106–112 (2019).
23. H. Ghiradella, Structure and development of iridescent butterfly scales: Lattices and laminae. *J. Morphol.* **202**, 69–88 (1989).
24. A. Dinwiddie *et al.*, Dynamics of F-actin prefigure the structure of butterfly wing scales. *Dev. Biol.* **392**, 404–418 (2014).
25. C. R. Day, J. J. Hanly, A. Ren, A. Martin, Sub-micrometer insights into the cytoskeletal dynamics and ultrastructural diversity of butterfly wing scales. *Dev. Dyn.* **248**, 657–670 (2019).
26. M. Stossberg, Die Zellvorgänge bei der Entwicklung der Flügelschuppen von *Ephestia kühniella* Z. *Z. Morphol. Ökol. Tiere* **34**, 173–206 (1938).
27. N. Paweletz, F. W. Schlote, Die Entwicklung der Schmetterlingsschuppe bei *Ephestia kühniella* Zeller. *Zeitschrift für Zellforschung* **63**, 840–870 (1964).
28. J. Overton, Microtubules and microfibrils in morphogenesis of the scale cells of *Ephestia kühniella*. *J. Cell Biol.* **29**, 293–305 (1966).
29. M. E. Greenstein, The ultrastructure of developing wings in the giant silkmoth, *Hyalophora cecropia*. II. Scale-forming and socket-forming cells. *J. Morphol.* **136**, 23–51 (1972).
30. H. Ghiradella, Development of ultraviolet-reflecting butterfly scales: How to make an interference filter. *J. Morphol.* **142**, 395–409 (1974).
31. V. Saranathan *et al.*, Structure, function, and self-assembly of single network gyroid (I4132) photonic crystals in butterfly wing scales. *Proc. Natl. Acad. Sci. U.S.A.* **107**, 11676–11681 (2010).
32. R. D. Reed, Evidence for Notch-mediated lateral inhibition in organizing butterfly wing scales. *Dev. Genes Evol.* **214**, 43–46 (2004).
33. A. F. Pomerantz *et al.*, Developmental, cellular and biochemical basis of transparency in clearwing butterflies. *J. Exp. Biol.* **224**, jeb237917 (2021).
34. B. D. Wilts *et al.*, Butterfly gyroid nanostructures as a time-frozen glimpse of intracellular membrane development. *Sci. Adv.* **3**, e1603119 (2017).

35. M. Iwata, Y. Ohno, J. M. Otaki, Real-time in vivo imaging of butterfly wing development: Revealing the cellular dynamics of the pupal wing tissue. *PLoS One* **9**, e89500 (2014).

36. Y. Ohno, J. M. Otaki, Live cell imaging of butterfly pupal and larval wings in vivo. *PLoS One* **10**, e0128332 (2015).

37. Y. Choi et al., Dynamic speckle illumination wide-field reflection phase microscopy. *Opt. Lett.* **39**, 6062–6065 (2014).

38. Y. Choi et al., Reflection phase microscopy using spatio-temporal coherence of light. *Optica* **5**, 1468–1473 (2018).

39. H. F. Nijhout, Ontogeny of the color pattern on the wings of *Precis coenia* (Lepidoptera: Nymphalidae). *Dev. Biol.* **80**, 275–288 (1980).

40. J. B. Nardi, S. M. Magee-Adams, Formation of scale spacing patterns in a moth wing: I. Epithelial feet may mediate cell rearrangement. *Dev. Biol.* **116**, 278–290 (1986).

41. R. Galant, J. B. Skeath, S. Paddock, D. L. Lewis, S. B. Carroll, Expression pattern of a butterfly achaete-scute homolog reveals the homology of butterfly wing scales and insect sensory bristles. *Curr. Biol.* **8**, 807–813 (1998).

42. F. Corson, L. Couturier, H. Rouault, K. Mazouni, F. Schweisguth, Self-organized Notch dynamics generate stereotyped sensory organ patterns in *Drosophila*. *Science* **356**, eaai7407 (2017).

43. H. Alawiye, E. Kuhl, A. Goriely, Revisiting the wrinkling of elastic bilayers I: Linear analysis. *Philos. Trans. R. Soc. Math. Phys. Eng. Sci.* **377**, 20180076 (2019).

44. K. Hirata, J. M. Otaki, Real-time in vivo imaging of the developing pupal wing tissues in the pale grass blue butterfly *Zizeeria maha*: Establishing the lycaenid system for multiscale bioimaging. *J. Imaging.* **5**, 42 (2019).

45. R. Zhou et al., Modeling the depth-sectioning effect in reflection-mode dynamic speckle-field interferometric microscopy. *Opt. Express.* **25**, 130–143 (2017).

46. K. Itoh, Analysis of the phase unwrapping algorithm. *Appl. Opt.* **21**, 2470 (1982).

47. R. M. Goldstein, H. A. Zebker, C. L. Werner, Satellite radar interferometry: Two-dimensional phase unwrapping. *Radio Sci.* **23**, 713–720 (1988).

48. A. D. McDougal, S. Kang, Z. Yaqoob, P. T. C. So, M. Kolle, Data and analysis codes for "In vivo visualization of butterfly scale cell morphogenesis in Vanessa cardui." Zenodo. https://doi.org/10.5281/zenodo.5532941. Deposited 10 November 2021.